SnSe₂ Quantum Dots: Facile Fabrication and Application in Highly Responsive UV-Detectors

Xiangyang Li [†], Ling Li *,[†], Huancheng Zhao, Shuangchen Ruan[ID], Wenfei Zhang, Peiguang Yan, Zhenhua Sun, Huawei Liang and Keyu Tao

Shenzhen Key Laboratory of Laser Engineering, College of Physics and Optoelectronic Engineering, Shenzhen University, Shenzhen 518060, China; 2170285209@email.szu.edu.cn (X.L.); 1800281011@email.szu.edu.cn (H.Z.); scruan@szu.edu.cn (S.R.); zhangwf@szu.edu.cn (W.Z.); yanpg@szu.edu.cn (P.Y.); szh@szu.edu.cn (Z.S.); hwliang@szu.edu.cn (H.L.); taokeyu@szu.edu.cn (K.T.)

* Correspondence: liling@szu.edu.cn; Tel.: +86-755-8653-2505

† These authors contributed equally to this work.

check for updates

Abstract: Synthesizing quantum dots (QDs) using simple methods and utilizing them in optoelectronic devices are active areas of research. In this paper, we fabricated SnSe₂ QDs via sonication and a laser ablation process. Deionized water was used as a solvent, and there were no organic chemicals introduced in the process. It was a facile and environmentally-friendly method. We demonstrated an ultraviolet (UV)-detector based on monolayer graphene and SnSe₂ QDs. The photoresponsivity of the detector was up to 7.5×10^6 mAW^{-1}, and the photoresponse time was ~0.31 s. The n–n heterostructures between monolayer graphene and SnSe₂ QDs improved the light absorption and the transportation of photocarriers, which could greatly increase the photoresponsivity of the device.

Keywords: SnSe₂ quantum dots; graphene; phototransistor; UV-detector

1. Introduction

Graphene-based electronic and optoelectronic devices have attracted extensive attention [1–3]. Mueller et al. demonstrated a vertical incidence metal–graphene–metal photodetector with an external responsivity of 6.1 mAW^{-1} at 1.55 μm [4]. The photoresponsivity was limited by the low absorption of the graphene. Quantum dots (QDs) can break this limitation. They can act as light absorption spots. The photo-induced carriers in them can transfer into the graphene film, and the charges in the graphene film transport to the electrodes quickly. Thus, the responsivity of a graphene-based device is improved [5–7]. Cheng et al. showed a phototransistor based on graphene and graphene QDs with a photoresponsivity of up to 4×10^{10} mAW^{-1}, but the response time was 10 s [8]. Sun et al. constructed an infrared photodetector based on graphene and PbS QDs with a responsivity of up to 10^{10} mAW^{-1} and a response time of 0.26 s [9]. Sun et al. demonstrated a UV phototransistor based on graphene and ZnSe/ZnS core/shell QDs. Its responsivity was up to 10^6 mAW^{-1} and the response time was 0.52 s [10].

In order to fabricate the QD solution with uniform distribution, the wet chemical method was commonly used. Some organic solvents, such as toluene or pyridine, were used in the process [9,10]. The chemical groups can cap the surface of the QDs and modify their charge transfer property, thus influencing the photo responsivity of the device. Synthesizing QDs using facile and green methods and utilizing them in optoelectronic devices are active areas of research.

Two-dimensional transition-metal dichalcogenides (TMDCs) have been applied in fluorescent imaging [11], biological sensing [12], and photocatalytic [13] due to their unique optoelectronic properties. Tin diselenide (SnSe₂) is a semiconductor in the TMDCs family. SnSe₂ QDs can be used in fast and highly responsive phototransistors since they have a tunable bandgap and high quantum

efficiency. In this paper, $SnSe_2$ QDs were fabricated via sonication and a laser ablation process. The deionized water was used as a solvent, and there were no organic chemicals introduced in the process. It was a facile and environmentally-friendly method. The phototransistor based on monolayer graphene and $SnSe_2$ quantum dots was demonstrated. The photoresponse time was ~0.31 s, and the photoresponsivity was up to 7.5×10^6 mAW^{-1}. The n–n heterostructures between monolayer graphene and $SnSe_2$ quantum dots enhance the light absorption and the generation of photocarriers. The photocarriers can transfer quickly from $SnSe_2$ QDs to graphene, thus improving the photoresponsivity of the device.

2. Experiment

SnSe$_2$ QDs were fabricated by sonication and the laser ablation process, as shown in Figure 1. The SnSe$_2$ bulk was bought from Six Carbon Technology. We put the SnSe$_2$ bulk in an agate mortar and manually ground it for 15 min to get SnSe$_2$ powders. Then, we dispersed 20 mg of powder in 30 mL of deionized water. The mixture was sonicated with a sonic tip for 2 h at the output power of 650 W in an ice-bath. The power was on for 4 s and off for 2 s. After sonication, the solution was a mixture of SnSe$_2$ small particles and flakes. The solution was transferred into a quartz cuvette and irradiated under a 1064 nm pulsed Nd:YAG laser for 10 min (6 ns, 10 Hz). The laser output power was 2.2 W. When the solution was irradiated by the laser pulses, the small particles and flakes absorbed the incident photon energies and formed extreme non-equilibrium conditions (high pressure and temperature) in a short time (~ns). After sustainable irradiation, the particles and nanosheets broke into tiny pieces. Then, the solution was centrifuged for 30 min at a speed of 6000 rpm. After that, the supernatant containing SnSe$_2$ QDs was collected.
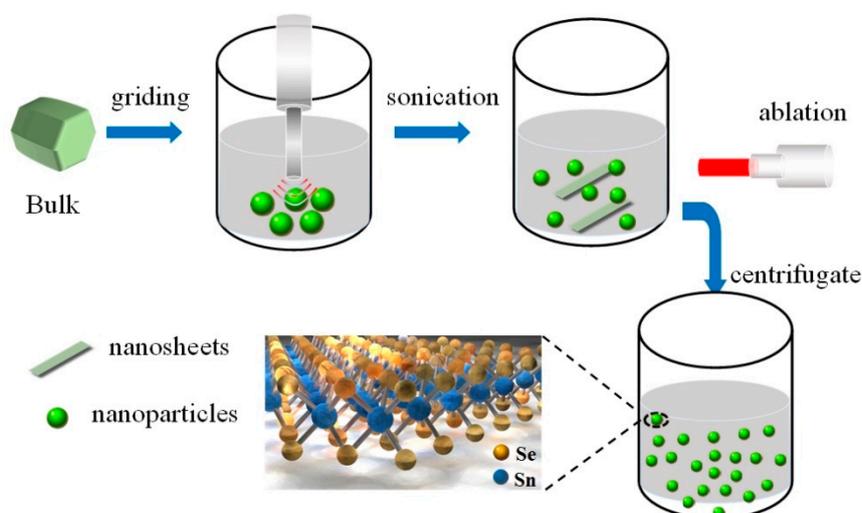

Figure 1. Schematic show of the SnSe$_2$ structure and the quantum dot (QD) fabrication process.

The morphology of the SnSe$_2$ QDs was studied using a high-resolution transmission electron microscope (TEM, FEI Tecnai G2 F30). The structure of the SnSe$_2$ QDs was characterized by X-ray diffraction spectroscopy (XRD, Bruker D8 Advance) and the Raman spectra (Horiba Labram HR Evolution). The absorption spectra were measured by a UV-vis spectrometer (Shimadzu UV-1700).

The chemical vapor deposition (CVD)-grown monolayer graphene was wet-transferred onto a p$^+$Si/SiO$_2$ substrate [14,15]. The thickness of SiO$_2$ was 285 nm. The highly doped p-type silicon served as the back-gate electrode. Then, the Cr/Au (10 nm/90 nm) source and drain electrodes were deposited on top of the graphene film by the thermal evaporation method. The channel length and width were 0.2 mm and 2 mm, respectively. The optoelectronic properties were studied using a probe station equipped with a semiconductor parameter analyzer (Keithley 4200). The illumination LED light wavelength was 405 nm.

3. Results and Discussion

Figure 2a shows the transmission electron microscope (TEM) image of $SnSe_2$ QDs as-fabricated. It shows an e- a size distribution in the range of 5–11 nm, and the average size is 9.8 nm, as indicated in Figure 2b. The average size of the QDs comes from the statistical analysis of the sizes of 200 QDs measured from TEM images. A high-resolution TEM image of a single $SnSe_2$ QD is shown in the inset of Figure 2a. The lattice spacing is about 0.33 nm, which corresponds to the (1010) planes of a hexagonal-phase $SnSe_2$ [16]. The result shows that the $SnSe_2$ QDs are crystalline.

(**a**)	(**b**)
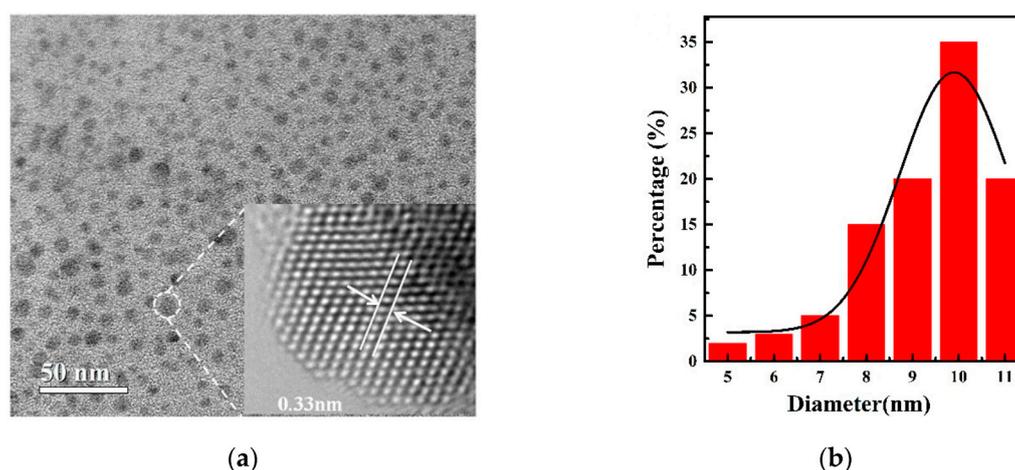
Figure 2. (**a**) TEM image of $SnSe_2$ QDs with a centrifugal speed of 6000 rpm. The inset shows the detailed crystal structure of a single QD; (**b**) the size distribution of the $SnSe_2$ QDs.

Figure 3a shows the XRD patterns of the $SnSe_2$ bulk and QDs. The $SnSe_2$ bulk has an obvious diffraction peak at $2\theta = 14.4°$ which corresponds to the (001) faces. In addition, some lower peaks located at $2\theta = 29.1°$, $2\theta = 31.2°$, $2\theta = 44.3°$, and $2\theta = 60.4°$ are assigned to the (002), (101), (003), and (004) faces. In $SnSe_2$ QDs, these diffraction peaks almost disappear except for a tiny peak at $2\theta = 29.1°$. After sonication and laser ablation, the $SnSe_2$ bulk was cracked into nanoparticles, and there was no constructive interference from the aligned crystal planes [13,17]. The tiny peak at $2\theta = 29.1°$ corresponds to the (002) face, which may come from the partial restacking of QDs in the process of drying. Figure 3b shows the Raman spectra of the $SnSe_2$ bulk and QDs. The incident laser wavelength is 514 nm and the spot size is around 2 μm. For the bulk $SnSe_2$, two Raman active vibration modes are observed at 110.3 cm^{-1} and 183.6 cm^{-1}, which correspond to the in-plane E_g and out-of-plane A_{1g} modes [18]. For the $SnSe_2$ QDs, the peak of the E_g mode is very weak, but the peak of the A_{1g} mode is observable and has a small blue-shift of ~1 cm^{-1}, which may be due to the surface effect and decrease of $SnSe_2$ thickness [19].

Figure 3c shows the absorption spectra for $SnSe_2$ QDs and $SnSe_2$ nanosheets solutions in the range of 250–1000 nm. The absorption band of the $SnSe_2$ nanosheets solution is broad, covering regions from the ultraviolet to near-infrared. It is similar to the absorption band reported for the $SnSe_2$ powders [20]. For the $SnSe_2$ QDs solution, only strong absorption from 250 nm to 420 nm is observed. The bulk $SnSe_2$ has an indirect bandgap of 1.0 eV [20]. When the particle size is reduced, the emergence of the quantum confinement effects leads to the discretization of energy levels. As a result, the $SnSe_2$ QDs show a larger band gap [21].
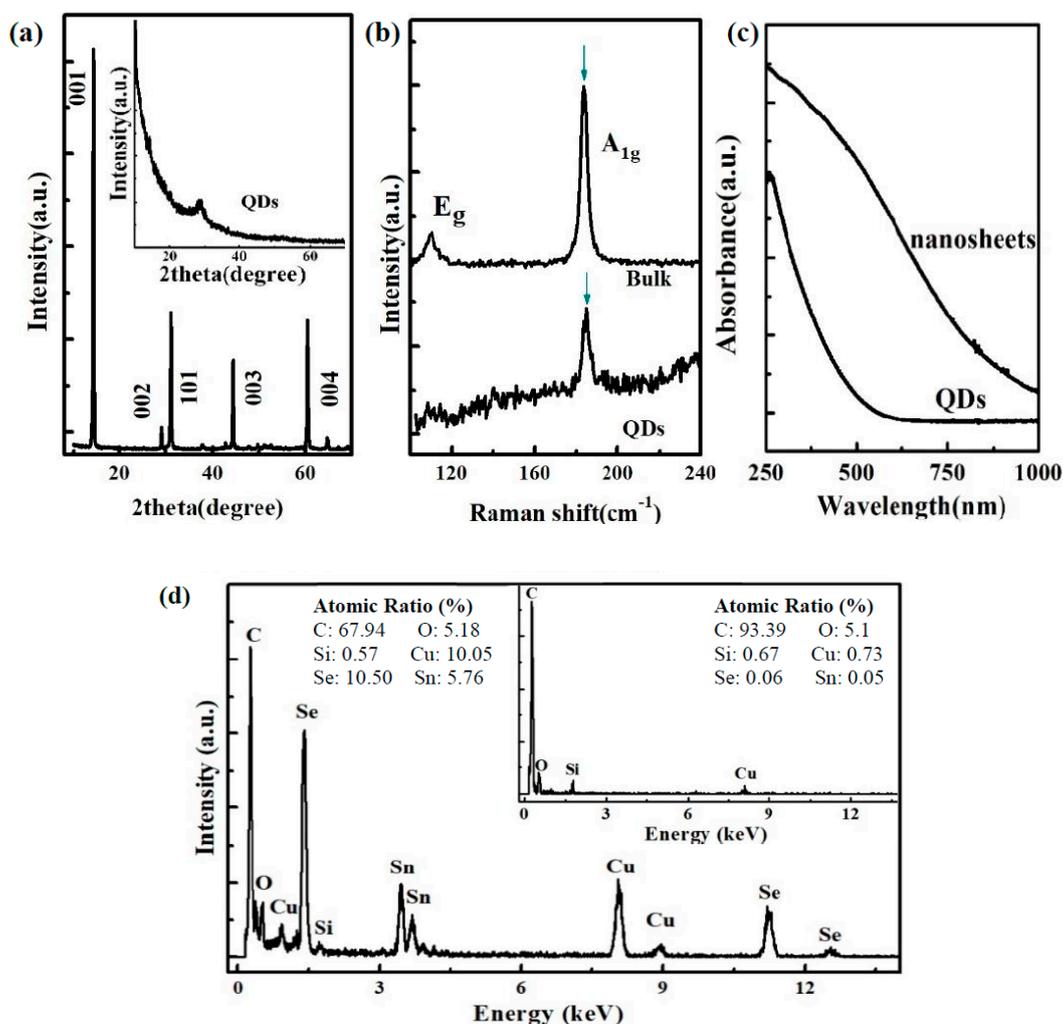
Figure 3. Spectroscopic characterizations. (**a**) XRD pattern of the SnSe$_2$ bulk and QDs; (**b**) Raman spectra of the SnSe$_2$ bulk and QDs; (**c**) absorption spectra of the SnSe$_2$ QDs and nanosheet solutions; (**d**) TEM energy dispersive spectra (TEM-EDS) of the SnSe$_2$ QDs. The inset shows the EDS of the TEM substrate without QDs.

Figure 3d shows the TEM energy dispersive spectra (TEM–EDS) of the SnSe$_2$ QDs. Tin and selenium can be clearly observed, and their atomic ratios are 5.76% (Sn) and 10.50% (Se), respectively. For comparison, the EDS of the TEM substrate (carbon film-coated copper grid without QDs) is shown in the inset of Figure 3d. The Cu, C, and Si signals come from the TEM grid and sample holder. The O peak arises from the oxygen adsorbed on the surface of the grid. The results show that the QDs are composed of tin and selenium.

Figure 4a schematically shows the photodetector decorated with SnSe$_2$ QDs on a p$^+$Si/SiO$_2$ substrate. The Raman spectra of the pure graphene on a p$^+$Si/SiO$_2$ substrate is shown in Figure 4b. Two Raman peaks at 1582 cm^{-1} (G line) and 2698 cm^{-1} (2D line) are observed. The ratio of the integrated intensities of the G line and 2D line is ~0.25. The peak at 1350 cm^{-1} (D line) in the spectra is very weak, indicating that the graphene is a monolayer with good quality. The I–V curves for the monolayer graphene phototransistor in the dark and with illumination under zero gate voltage (V$_G$ = 0 V) are shown in Figure 4c. The illumination density is 350 μW/cm^2. As shown in the figure, there is no change between the current in the dark and under illumination, indicating that the photoresponse of pure graphene is negligible.
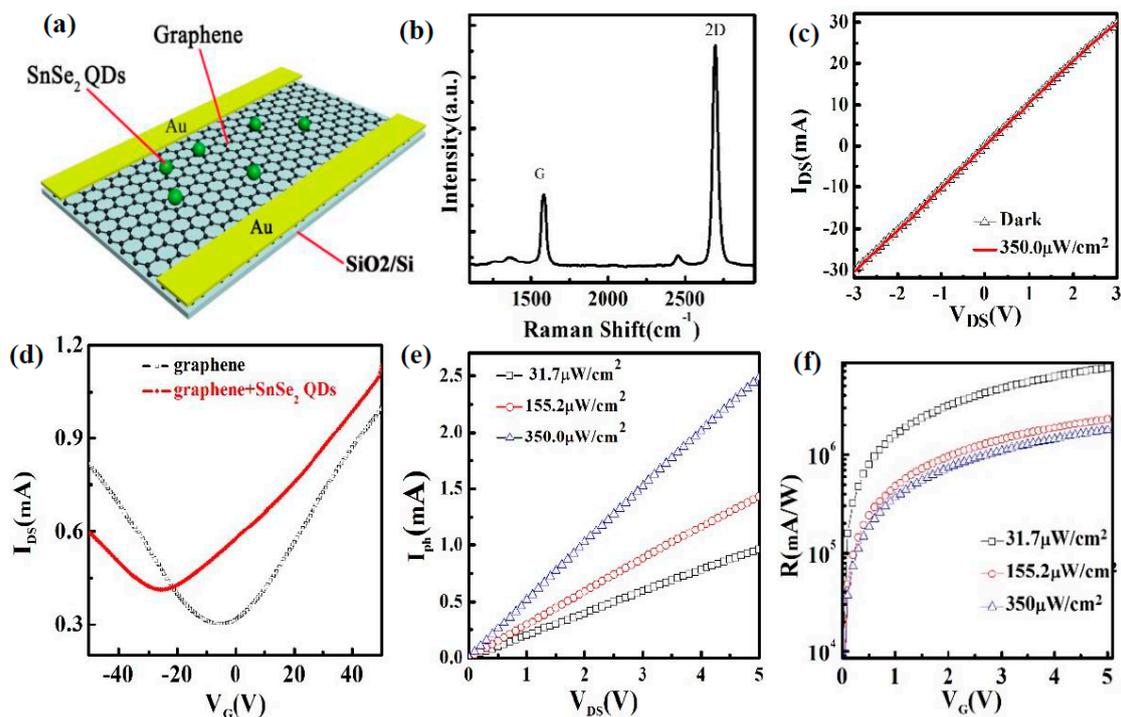
Figure 4. (**a**) Schematic diagram of a graphene photodetector decorated with $SnSe_2$ QDs; (**b**) Raman spectra of the pure graphene on a p^+Si/SiO_2 substrate; (**c**) the I–V curves for the single-layer graphene phototransistor in the dark and with illumination under zero-gate voltage (V_G = 0 V); (**d**) transfer characteristics (I_{DS}-V_G, V_{DS} = 0.5 V) of the phototransistor with and without $SnSe_2$ QDs on the graphene film; (**e**) photocurrent and (**f**) responsivity of a $SnSe_2$ QD-decorated graphene photodetector as functions of drain voltages at different illumination densities. The illumination wavelength is 405 nm.

Figure 4d shows the transfer curves (I_{DS}-V_G, V_{DS} = 0.5 V) of the device with and without $SnSe_2$ QDs in which the light is absent. The transfer curve of the device without $SnSe_2$ QDs exhibits a typical V-shape. The field-effect mobilities are ~230 $cm^2V^{-1}s^{-1}$ for electrons and ~220 $cm^2V^{-1}s^{-1}$ for holes. The negative, neutral charge point (about −5 V) of single-layer graphene is observed in Figure 4d, indicating an electron dominated conduction in the graphene. The same behavior was also observed by Sun et al. [10]. Graphene is very sensitive to the surroundings. The defects in the SiO_2 substrate, residues from processing and handling, charged impurities, and substrate surface roughness can cause the shift of the neutral charge point [22]. The $SnSe_2$ QDs solution was dropped on the top of graphene film and heated at 40 °C for 30 min in a glove box filled with N_2 gas. The transfer curve of the photodetector with $SnSe_2$ QDs becomes asymmetric, and the Dirac point converts to a negative gate voltage (about −22 V). The shift indicates that the $SnSe_2$ QDs are n-type semiconductors, which are the same type as the bulk $SnSe_2$ [20]. The electron and hole mobilities decrease to ~160 $cm^2V^{-1}s^{-1}$ and ~130 $cm^2V^{-1}s^{-1}$, respectively.

In order to study the optoelectronic properties of the device, we measured the photocurrents at different illumination densities with zero gate voltage (V_G = 0 V). Figure 4e shows the relationship between the photocurrent ($I_{Ph} = I_{Light} − I_{Dark}$) and the applied drain voltages. I_{Light} is the drain current under illumination, and I_{Dark} is the drain current without illumination. The photocurrent increases while increasing the illumination density. Figure 4f represents the responsivity ($R = I_{ph}/(WLE_e)$) of the photodetector as functions of drain voltages at different illumination densities. The responsivity decreases while increasing the illumination density, which is consistent with the reported UV-detectors [23]. The maximum responsivity of the device is about 7.5×10^6 mAW^{-1} (V_{DS} = 5 V) at an incident power density of 31.7 $\mu W/cm^2$, which is higher than that reported in graphene-based UV phototransistors [24–26].

Figure 5a shows the transfer curves of the photodetector at different illumination densities. The Dirac point of the device shifts to a lower negative gate voltage while increasing illumination density. The shift of the transfer curves (ΔV_G) is plotted as a function of illumination densities in Figure 5b. The shift of the transfer curve (ΔV_G) changes linearly with the light illumination density (Ee), indicating that the photo-induced carrier density in $SnSe_2$ QDs increases with increasing illumination density. This illumination density-dependent shift does not appear in the pure graphene phototransistor. The existence of $SnSe_2$ QDs leads to this photoresponse behavior. As shown in Figure 5a, the electron mobility in the $SnSe_2$ QD-decorated device is higher than that of holes at different illumination densities. The photo-induced electron-hole pairs are separated at the interface between $SnSe_2$ QDs and monolayer graphene. The $SnSe_2$ QDs/graphene heterojunction facilitates the injection of photo-generated electrons from $SnSe_2$ QDs into the graphene, leading a local n-doping in the graphene channel. Since the transfer rate of holes is lower that of electrons, net positive charges remain in the $SnSe_2$ QDs. Then, a lower negative gate voltage is required to obtain the charge neutral point (Dirac point) in the detector. A similar process was reported in a p-doped graphene/PbS QDs phototransistor by Sun et al. [9].
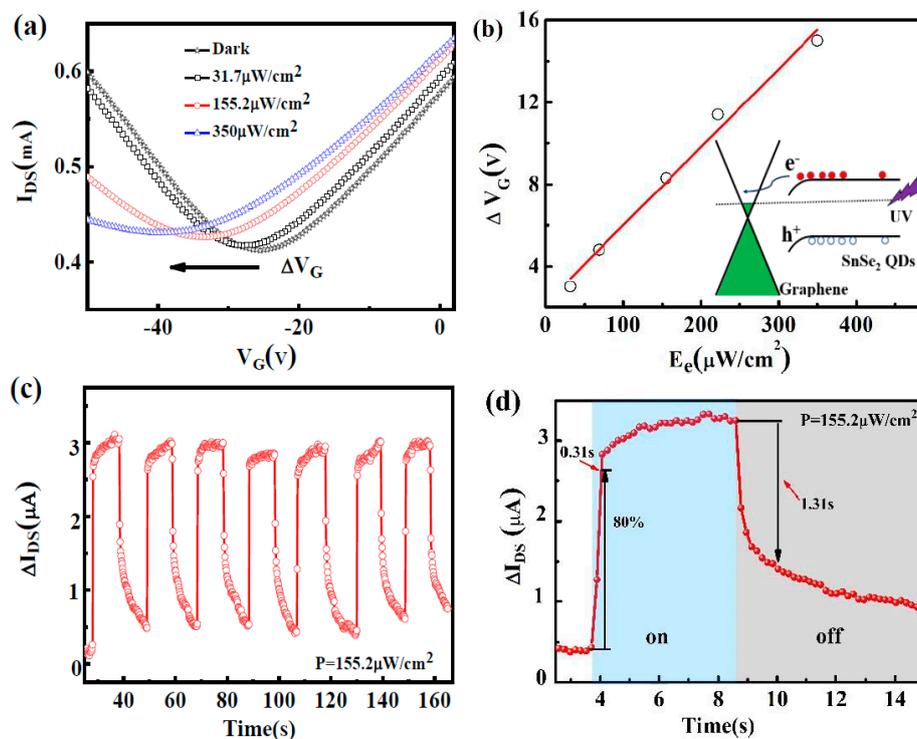

Figure 5. (**a**) Transfer characteristics of a graphene photodetector decorated with $SnSe_2$ quantum dots at different illumination densities (wavelength: 405 nm, $V_{DS} = 0.5$ V); (**b**) horizontal shift of transfer curves as functions of illumination densities. The inset shows the charge transfer between $SnSe_2$ QDs and graphene; (**c**) current response to on/off light illumination for several cycles; (**d**) photocurrent response time of the device. ($V_{DS} = 0.05$ V, illumination density: 155.2 μW/cm ^{2}).

Figure 5c shows the current response to on/off light illumination and Figure 5d shows the photocurrent response time of the device ($V_G = 0$ V, $V_{DS} = 0.05$ V, illumination density: 155.2 μW/cm^2). The photocurrent increases with time when the illumination is on and decreases with time when the illumination is off. As shown in Figure 5d, the photocurrent increases to 80% with a response time of 0.31 s, which is faster than that reported in graphene devices [9,10,24,26,27]. The response time includes charge generation time, charge transfer time in heterojunctions, and charge collection time. In our experiment, the measured graphene charge mobility is smaller than the value for perfect graphene (up to 200,000 $cm^2V^{-1}s^{-1}$), which may be due to the defects induced in the graphene film

while transferring to the substrate, and the response time can be improved by optimizing the graphene transfer process. When the light is turned out, the photocurrent decreases to 20% with a time of 1.31 s.

The photocurrent of the detector is influenced by the $SnSe_2$ QDs density. We have measured the AFM pictures and photocurrents for detectors with different $SnSe_2$ QDs densities. As shown in Figure 6, the photocurrent increases with an increase of the $SnSe_2$ QDs density under the same irradiation density (illumination density: 350 $\mu W/cm^2$). When the $SnSe_2$ QDs thickness is larger than 40 nm, the photocurrent tends to decrease, which may be due to the decrease of the charge transfer between the QDs layers.
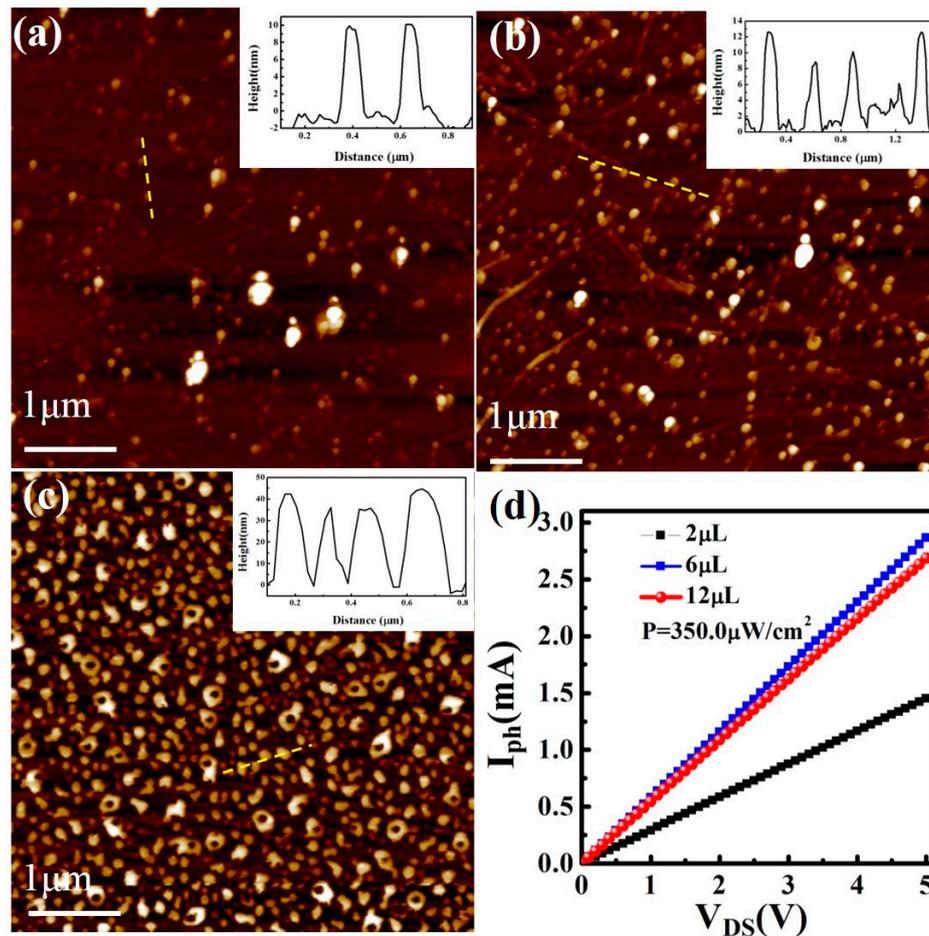
Figure 6. The AFM images of $SnSe_2$ QDs with different densities (**a**) 2 μL, (**b**) 6 μL, and (**c**) 12 μL. The insets show their height profiles. (**d**) The photocurrents with different $SnSe_2$ QDs densities at the irradiation density of 350.0 $\mu W/cm^2$.

4. Conclusions

In summary, uniformly distributed $SnSe_2$ quantum dots were synthesized at room temperature using a facile and environment-friendly method. The UV-detector based on monolayer graphene and $SnSe_2$ quantum dots was demonstrated. The device showed fast photoresponse time of ~0.31 s, and its photoresponsivity was up to 7.5×10^6 mAW^{-1}. The n–n heterostructures between monolayer graphene and $SnSe_2$ QDs improved the light absorption and the transportation of photocarriers, which have promising applications in optoelectronic devices.

References

1. Bonaccorso, F.; Sun, Z.; Hasan, T.; Ferrari, A.C. Graphene Photonics and Optoelectronics. *Nat. Photonics* **2010**, *4*, 611–622. [CrossRef]

2. Xia, F.; Thomas, M.; Lin, Y.; Valdes, Y.; Phaedon, A. Ultrafast Graphene Phototransistor. *Nat. Nanotechnol.* **2009**, *4*, 839–843. [CrossRef] [PubMed]

3. Li, X.; Li, T.; Chen, Z.; Fang, H.; Li, X.; Wang, X.; Xu, J.; Zhu, H. Graphene and Related Two-Dimensional Materials: Structure-Property Relationships for Electronics and Optoelectronics. *Appl. Phys. Rev.* **2017**, *4*, 021306. [CrossRef]

4. Mueller, T.; Xia, F.; Phaedon, A. Graphene Phototransistors for High-Speed Optical Communications. *Nat. Photonics* **2010**, *4*, 297–301. [CrossRef]

5. Li, X.M.; Zhu, H. The Graphene–Semiconductor Schottky Junction. *Phys. Today* **2016**, *69*, 46–51. [CrossRef]

6. Liu, C.; Chang, Y.; Theodore, B.; Zhong, Z. Graphene Phototransistors with Ultra-Broadband and High Responsivity at Room Temperature. *Nat. Nanotechnol.* **2014**, *9*, 273–278. [CrossRef] [PubMed]

7. Fitzmorris, B.; Pu, Y.; Jason, K.; Lin, Y.; Hu, Y.; Li, U.; Zhang, J. Optical Properties and Exciton Dynamics of Alloyed Core/Shell/Shell $Cd_{1-X}Zn_xSe/ZnSe/ZnS$ Quantum Dots. *ACS Appl. Mater. Interfaces* **2013**, *5*, 2893–2900. [CrossRef]

8. Cheng, S.; Weng, T.; Lu, M.; Tan, W.; Chen, J.; Chen, Y. All Carbon-Based Phototransistors: An Eminent Integration of Graphite Quantum Dots and Two Dimensional Graphene. *Sci. Rep.* **2013**, *3*, 2694. [CrossRef]

9. Sun, Z.; Liu, Z.; Li, J.; Tai, G.; Lan, S.; Yan, F. Infrared Phototransistors Based on CVD-Grown Graphene and PbS Quantum Dots with Ultrahigh Responsivity. *Adv. Mater.* **2012**, *24*, 5878–5883. [CrossRef]

10. Sun, Y.; Dan, X.; Sun, M.; Teng, C.; Liu, Q.; Chen, R.; Lan, X.; Ren, T. Hybrid Graphene/Cadmium-Free ZnSe/ZnS Quantum Dots Phototransistors for UV Detection. *Sci. Rep.* **2018**, *8*, 1–8. [CrossRef]

11. Long, H.; Li, T.; Chun, P.; Chun, Y.; Kin, H.; Yang, C.; Tsang, Y. The WS_2 Quantum Dot: Preparation, Characterization and Its Optical Limiting Effect in Polymethylmethacrylate. *Nanotechnology* **2016**, *27*, 414005. [CrossRef] [PubMed]

12. Han, Y.; Zhang, C.; Gu, W.; Ding, C.; Li, X.; Xian, Y. Facile Synthesis of Water-Soluble WS_2 Quantum Dots for Turn-on Fluorescent Measurement of Lipoic Acid. *J. Phys. Chem. C* **2016**, *120*, 12170–12177.

13. Xu, S.; Li, D.; Wu, P. One-Pot, Facile, and Versatile Synthesis of Monolayer MoS_2/WS_2 Quantum Dots as Bioimaging Probes and Efficient Electrocatalysts for Hydrogen Evolution Reaction. *Adv. Funct. Mater.* **2015**, *7*, 1127–1136. [CrossRef]

14. He, R.; Peng, L.; Liu, Z.; Zhu, H.; Zhao, X.; Chan, H.; Yan, F. Solution-Gated Graphene Field Effect Transistors Integrated in Microfluidic Systems and Used for Flow Velocity Detection. *Nano Lett.* **2012**, *12*, 1404–1409. [CrossRef] [PubMed]

15. Chiang, C.W.; Haider, G.; Tan, W.C.; Chen, Y.F. Highly Stretchable and Sensitive Photodetectors Based on Hybrid Graphene and Graphene Quantum Dots. *ACS Appl. Mater. Interfaces.* **2016**, *8*, 466–471. [CrossRef] [PubMed]

16. Zhou, X.; Lin, G.; Tian, W.; Zhang, Q.; Jin, S.; Li, H.; Yoshio, B.; Dmitri, G.; Zhai, T. Ultrathin $SnSe_2$ Flakes Grown by Chemical Vapor Deposition for High-Performance Phototransistors. *Adv. Mater.* **2015**, *27*, 8035–8041. [CrossRef]

17. Zankat, C.; Pratik, P.; Solanki, G.K.; Patel, K.V.; Pathak, M.; Som, N.; Prafulla, J. Investigation of Morphological and Structural Properties of V Incorporated $SnSe_2$ Single Crystals. *Mater. Sci. Semicond. Process.* **2018**, *8*, 137–142. [CrossRef]

18. Zhou, W.; Yu, Z.; Song, H.; Fang, R.; Wu, Z.; Li, L.; Ni, Z.; Wei, R.; Lin, W.; Ruan, S. Lattice Dynamics in Monolayer and Few-Layer $SnSe_2$. *Physcal Rev. B* **2017**, *96*, 035401. [CrossRef]

19. Qiao, X.; Wu, J.; Zhou, L.; Qiao, J.; Shi, W.; Chen, T.; Zhang, X.; Zhang, J.; Ji, W.; Tan, P.H. Polytypism and Unexpected Strong Interlayer Coupling of Two-Dimensional Layered ReS_2. *Adv. Funct. Mater.* **2015**, *8*, 8324–8332. [CrossRef]

20.   Borges, Z.V.; Poffo, C.M.; de Lima, J.C.; de souza, S.M.; Trichês, D.M.; Nogueira, T.P.O.; Manzato, L.; de Biasi, R.S. Study of Structural, Optical and Thermal Properties of Nanostructured SnSe$_2$ Prepared by Mechanical Alloying. *Mater. Chem. Phys.* **2016**, *169*, 47–54. [CrossRef]

21.   Solati, E.; Laya, D.; Davoud, D. Effect of Laser Pulse Energy and Wavelength on the Structure, Morphology and Optical Properties of ZnO Nanoparticles. *Opt. Laser Technol.* **2014**, *58*, 26–32. [CrossRef]

22.   Kathalingam, A.; Senthilkumar, V.; Rhee, J.-K. Hysteresis I-V nature of mechanically exfoliated graphene FET. *J. Mater. Sci. Mater. Electron.* **2014**, *25*, 1303–1308. [CrossRef]

23.   Cheng, W.; Tang, L.; Xiang, J.; Ji, R.; Zhao, J. An Extreme High-Performance Ultraviolet Photovoltaic Detector Based on Zno Nanorods/Phenanthrene Heterojunction. *RSC Adv.* **2016**, *6*, 12076–12080. [CrossRef]

24.   Babichev, A.V.; Zhang, H.; Pierre, L.; Julien, F.H.; Egorov, Y.; Lin, Y.; Tu, L.; Maria, T. Gan Nanowire Ultraviolet Phototransistor with a Graphene Transparent Contact. *Appl. Phys. Lett.* **2013**, *103*, 201103. [CrossRef]

25.   Boruah, B.; Anwesha, M.; Abha, M. Sandwiched Assembly of Zno Nanowires between Graphene Layers for a Self-Powered and Fast Responsive Ultraviolet Phototransistor. *Nanotechnology* **2016**, *27*, 095205. [CrossRef] [PubMed]

26.   Lu, Y.; Wu, Z.; Xu, W.; Lin, S. ZnO Quantum Dot-Doped Graphene/H-BN/Gan-Heterostructure Ultraviolet Phototransistor with Extremely High Responsivity. *Nanotechnology* **2016**, *26*, 48LT03. [CrossRef] [PubMed]

27.   Tang, J.; Kyle, K.; Sjoerd, H.; Kwang, J.; Liu, H.; Larissa, L.; Melissa, F.; Wang, X.; Ratan, D.; Dongkyu, C.; et al. Colloidal-Quantum-Dot Photovoltaics Using Atomic-Ligand Passivation. *Nat. Mater.* **2011**, *10*, 765–771. [CrossRef] [PubMed]